Nickel doped zinc oxide with improved photocatalytic activity for Malachite Green Dye degradation and parameters affecting the degradation

K. Nomita Devi[1,*] (iD), Sh. Anju Devi[1], W. Joychandra Singh[1], and K. Jugeshwar Singh[2]

[1] *Department of Physics, Manipur University, Canchipur, Imphal 795003, India*
[2] *Talent Development Centre, Indian Institute of Science, Kudapura, Karnataka 577536, India*

ABSTRACT

$Zn_{1-x}Ni_xO$ ($x = 0$, 0.02, 0.04, 0.06, 0.08, 0.1) was synthesized successfully using chemical co-precipitation method. The structural, morphological and optical properties of the synthesized samples were investigated using XRD (X-ray diffraction), SEM (scanning electron microscope), EDX (energy-dispersive X-ray), TEM (transmission electron microscope), FTIR (Fourier transform infrared) and UV–Vis spectroscopy. The photocatalytic activities of the synthesized samples toward the degradation of Malachite Green (MG) dye under UV light irradiation were studied. $Zn_{0.94}Ni_{0.06}O$ was observed to be the better photocatalyst among the studied samples which degrades 77% of the dye under 4 h of irradiation. The effect of operational parameters such as catalyst dosage, initial dye concentration and pH on the degradation percentage was investigated. An optimum condition was obtained for a catalyst load of 0.10 g/L into 15 ppm dye solution at pH 9 which degrades 76% of the dye under 1hour of UV irradiation. Reusability test of the photocatalyst was also performed to check the stability for long-term application of the samples.

1 Introduction

Although the availability of clean and potable water is a must for mankind and other living beings, its scarcity is one of the major problems that the world is facing today. Several industries and factories such as textiles, food colouring, cosmetics, paper and leather dispose their effluents in the water. Globally, every year, 1–20% of the dyes produced are discharged into the water bodies which makes the water unfit for consumption since even very little concentration of dye can affect water to a great extent [1]. As a result, there is an urgent requirement to develop an economic and ecofriendly technique for water purification. Among the various techniques adopted commonly such as coagulation, flocculation, sedimentation and photocatalysis, photocatalysis is one of the most efficient and low cost method. The

Address correspondence to E-mail: kongkhamn@gmail.com

advantages of this process include low energy consumption, non-toxicity and ability to utilize solar energy which is the most abundant form of energy [2, 3].

In recent years, nanosized-inorganic semiconductor materials, such as TiO_2, ZnO, ZnS, CdS, WO_3 have gained considerable research interest as photocatalyst. Zinc oxide (ZnO) is one of the most widely studied photocatalysts owing to its properties such as wide band gap energy (3.2 eV), large exciton binding energy of 60 meV [4], ability to absorb large range of solar spectrum, environmental friendliness, etc. However, the photocatalytic efficiency of ZnO gets affected to a great extent due to the rapid recombination of the generated charge carriers. Among the strategies for overcoming the limitation of charge carrier recombination, doping with transition metals is an effective way which will facilitate the efficient transportation and separation of electron–holes by introducing energy levels in between the conduction and valence band of the nanostructure [5–7]. This strategy modifies the electronic configuration of the photocatalyst where the generated electron–hole pair will be trapped thereby restricting their recombination.

There have been various reports on the improved photocatalytic performance of ZnO doped with nickel. J. Zhao et al. investigated the photocatalytic efficiency of $Zn_{1-x}Ni_xO$ ($x = 0$, 0.02, 0.05, 0.10) nanorods synthesized by hydrothermal method for the degradation of Rhodamine B under UV light irradiation and reported that 5% Ni doped ZnO exhibited the highest photocatalytic activity in degrading the dye [8]. S. M. Mousavi et al. synthesized Ni doped ZnO hollow spheres in an ultrasonic bath at a low template fructose for degrading Congo Red (CR) as an Azo dye under visible light. According to the results, Ni–ZnO hollow spheres outperform the pure ZnO hollow spheres in terms of the photocatalytic activities. 3% Ni doped ZnO was observed to be the most effective photocatalyst by achieving almost complete degradation after 80 minutes of irradiation time [9]. S. Kant et al. prepared pure ZnO and 5% Ni doped ZnO using sol–gel technique [10]. The photocatalytic efficiency of the prepared nanostructures was investigated for the degradation of methylene blue dye under visible light irradiation and reported around 60% degradation of the dye in 90 min by doped ZnO. A.K. Azfar et al. studied and compared the photo catalytic
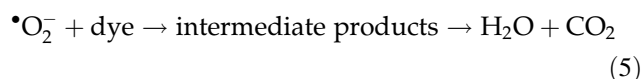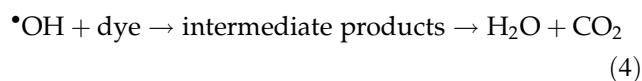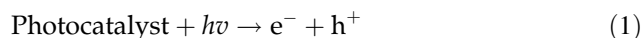
activity of Ag and Ni doped ZnO prepared by sol–gel method towards the degradation of methyl orange dye under UV light irradiation [11]. Ag doped ZnO showed good photocatalytic efficiency but Ni doped ZnO showed low photocatalytic efficiency with 1% Ni doped ZnO giving the best outcomes of 31.68% degradation after 120 min of UV irradiation. Though these studies show remarkable improvement in the photocatalytic performance of ZnO after doping with Ni, significant issues with these works were either synthesis process adopted requires high calcination temperatures, long duration, high energy consumption or slow degradation kinetics. Moreover, the efficiency of the photocatalytic system is also highly dependent on a number of operational parameters that govern the photodegradation of the organic molecule. The photodegradation depends on some basic parameters such as initial dye concentration, amount of photocatalyst, pH of the solution which were not investigated in most of the earlier works.

Most of the studies lack the combined information of a simple, cost effective, low energy utilization synthesis technique and effect of operational parameters on photocatalysis process. In the present work we have synthesized an efficient Ni doped ZnO photocatalyst with different percentage of doping using a simple and low cost Co precipitation method for the photocatalytic degradation of MG dye. Experiments were performed by changing the operational parameters such as catalyst loading, initial dye concentration and pH for obtaining the optimum degradation of dye. To the best of the authors' knowledge, an indepth study on the degradation of MG dye by Ni doped ZnO under the same experimental conditions has not been reported earlier. The effect of different experimental conditions on the degradation process was also investigated.

1.1 Basic mechanism of photocatalysis

The concept and mechanism of photocatalysis have been explained and discussed by numerous researchers [12–14]. When light, having energy greater than the band gap energy of the semiconductor material, falls on the material surface, electron from the valence band gets excited to the conduction band creating a hole in the valence band. The generated electron and hole combine with O_2 and H_2O forming oxygen and hydroxyl radical which in turn reacts with the dyes and degrade them into harmless

CO_2 and H_2O. The reactions involved in the process are described as follows:

$$Photocatalyst + h\nu \rightarrow e^- + h^+ \tag{1}$$

$$e^- + O_2 \rightarrow {}^\bullet O_2^- \tag{2}$$

$$h^+ + OH^- \rightarrow {}^\bullet OH \tag{3}$$

$${}^\bullet OH + dye \rightarrow intermediate\ products \rightarrow H_2O + CO_2 \tag{4}$$

$${}^\bullet O_2^- + dye \rightarrow intermediate\ products \rightarrow H_2O + CO_2 \tag{5}$$

2 Experimental details

2.1 Synthesis

Analytical grade purity chemicals were used without further purification. Zinc nitrate hexahydrate [$Zn(NO_3)_2 \cdot 6H_2O$] (Merck, 98%) and nickel nitrate hexahydrate [$Ni(NO_3)_2 \cdot 6H_2O$] (Merck, 98%) were used as the precursors for Zn and Ni atoms, respectively. Double distilled water was used as solvent in the synthesis process. Sodium hydroxide (NaOH) (Merck, 98%) was used as a precipitating agent.

In a typical synthesis of $Zn_{1-x}Ni_xO$ (x = 0.00, 0.02, 0.04, 0.06, 0.08, 0.1) by simple wet chemical co-precipitation method, the appropriate amount of zinc nitrate and nickel nitrate was completely dissolved in 200 ml of distilled water. The mixture solution was kept under constant stirring of 600 rpm for 15 min on a magnetic stirrer in order to mix the solution uniformly. After complete dissolution of the mixture, freshly prepared 0.1 M NaOH solution was added drop by drop until the pH of the solution becomes 11 and then stirred for 2 h to complete the reaction. The precipitate formed was washed with distilled water for several times in order to remove any other soluble impurities present and then filtered followed by drying at 80 °C for 24 h during which the hydroxide phase was converted into oxide phase. The final product was then ground to obtain the fine powder.

2.2 Characterization

The structural characterization of the synthesized samples was done by using Phillip's PanAnalytical X'pert pro diffractometer with Cu target ($\lambda = 1.5405$ Å) in the 2θ range of 20°–80°. The instrumental broadening including instrumental symmetry was calibrated using Si standard sample. The morphology and chemical composition of the samples was studied using Scanning electron microscope (FEI Quanta 250) equipped with an energy-dispersive X-ray spectrometer (EDX-Quanta 250). The transmission electron microscopy (TEM) analysis was done using FEI Tecnai T20-S. Fourier transform infrared (FTIR) spectra were recorded in an FTIR spectrometer (Shimadzu 8400S). FTIR spectra were obtained using pressed pellets of the prepared samples in potassium bromide (KBr) in the wavenumber range of 400 cm^{-1} to 4000 cm^{-1} with a resolution of 4 cm^{-1}. The optical absorption spectrum was measured using Ocean optics UV–Visible spectrophotometer (HR4000).

2.3 Photocatalysis

Photocatalysis experiment was performed in a custom made reactor which includes a magnetic stirrer and a UV lamp. The photocatalytic activities of $Zn_{1-x}Ni_xO$ (x = 0.00, 0.02, 0.04, 0.06, 0.08, 0.10) were investigated towards the degradation of MG dye solution under the irradiation of 8 W (UV-C, 254 nm) Mercury lamp (Phillips). In a typical experiment, 10 mg of the photocatalyst was added into 100 ml of dye solution. It was kept under dark for 1hr to attain adsorption–desorption equilibrium after which it was irradiated with UV light. Approximately 5 ml of irradiated solutions was taken out after a regular time interval of 30 min each and the photocatalytic activity was monitored by measuring the absorption spectra of the solution.

3 Results and discussion

3.1 Structural analysis

Figure 1 shows the XRD patterns for the undoped and Ni doped ZnO samples with different doping percentage. Using X'Pert High Score plus software, the observed XRD patterns were indexed as hexagonal wurtzite structure of ZnO which are in good agreement with the ICDD Reference Pattern: zinc oxide, 01-079-2205. In the diffraction pattern of the doped samples, no additional peak corresponding to metal Ni and its oxides phases were observed which reveals that the Ni atoms successfully replaced the Zn

atoms from the lattice sites of ZnO without disturbing the wurtzite structure of ZnO. The average grain size of the Ni doped and undoped sample was calculated using Debye–Scherrer formula [15].

$$g = \frac{0.9\lambda}{\beta\cos\theta},\tag{6}$$

where g is the grain size, $\lambda = 1.5405\,\text{Å}$ for Cu K_α radiation, β is the Full width at half maximum and θ is the Bragg's diffraction angle. The grain size of the undoped sample is 31 nm which decreases to 28 nm for $x = 0.04$. With increase in doping concentration, the grain size increases from 30 nm for $x = 0.06$ to 33 nm for $x = 0.1$. This variation in grain size shows that the growth and nucleation of the doped samples increases when $x > 0.06$. Many researchers had also reported the increase in grain size when the doping concentration in TM doped ZnO and other metal oxides was high [16, 17].

The Rietveld Refinement analysis of the XRD patterns of the series of $Zn_{1−x}Ni_xO$ was also performed with the help of Fullprof Suite program using the $P63mc$ (No. 186) space group [18]. A typical Rietveld refined plot of ZnO sample is shown in Fig. 2. It is observed from Fig. 2 that the profile for the observed XRD pattern is well matched with the calculated pattern of the space group $P63mc$. During the refinement of the pattern, the Pseudo-Voigt peak shape function was utilized to refine the several parameters. The parameters, scale factor, zero shifting and six background co-efficient were refined in the first step. In the next step, the lattice parameter, profile shape, width of the peak, preferred orientation, global thermal factor, asymmetric factor and atomic co-ordinate of oxygen were refined in sequence. The atomic co-ordinates of the zinc were taken as the fixed parameter. Other factors like isothermal parameter and occupancies of both zinc and oxygen were also taken as fixed during the refinement.

The obtained refined parameters such as three lattice parameter, cell volume, atomic fractional position, the reliability factor $\left(R_p, R_{wp}, R_{exp}, R_{Bragg} \text{ and } R_F\right)$ and goodness of the fitting (χ^2) are reported in Table 1. The data revealed a slight decreasing pattern in lattice parameter, a and
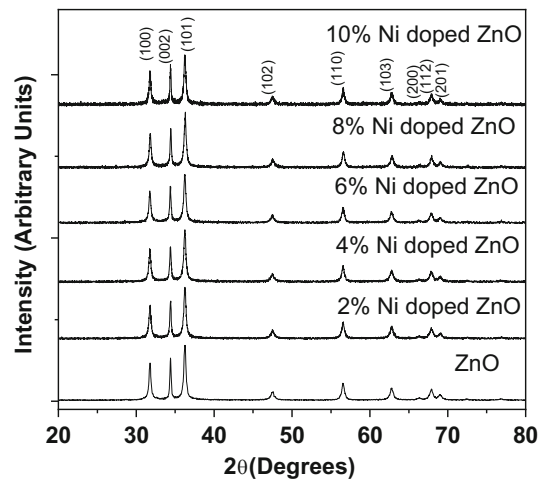

Fig. 1 XRD diffraction pattern of Ni doped and undoped ZnO

c with doping of Ni concentration. The values of c/a remain almost constant.

In tetrahedral arrangement, the ionic radii of Zn^{2+} and Ni^{2+} are 0.60 Å and 0.55 Å, respectively. The slight decrease in lattice parameters with doping is attributed to the linear mismatch in ionic radius of dopant $Ni^{2+}$and host Zn^{2+} atoms. The unit cell volume is also decreased with doping concentration because of decreased lattice parameter. The slight higher value of $R_{Factors}$ is due to the nanocrystalline nature of the sample and such higher value was also reported by many researchers [19–22]. However, the low value of the χ^2 indicates goodness of the fitting and a good agreement between the refined and observed XRD patterns for the wurzite ZnO.

3.2 Morphological and chemical compositional analysis

Figure 3a–f shows the SEM images of undoped and doped ZnO samples. It is evident from the images that undoped ZnO possess a distinct spindle shaped morphology of average diameter of 290 nm and length of 490 nm and the particles are well separated and distributed uniformly. With the incorporation of Ni atoms, the spindle shaped morphology of the samples was affected and a few spherical shape particles are seen dispersed. The dispersion of spherical particles increases with the increase in Ni concentration in the samples. The diameter and length of the spindle shaped particles for doped samples are found to be in the range of 130–240 nm
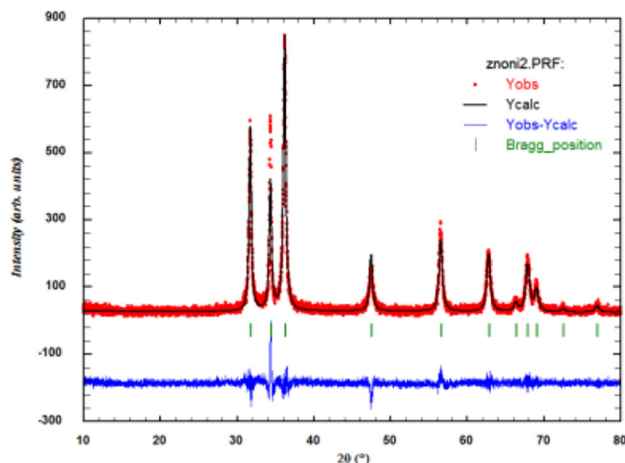
Fig. 2 A typical Rietveld refined XRD pattern of ZnO sample

and 175–390 nm, respectively. The average size of the dispersed spherical shaped particles ranges between 60 and 150 nm. Figure 4a–c shows the EDX spectrum for undoped ZnO, 4% doped and 10% Ni doped ZnO. The EDX image of undoped ZnO shows the emission of X-ray corresponding to oxygen and zinc atoms only. The quantitative analysis confirms the presence of Zn and O atoms as per their nominal stoichiometry. The presence of Ni atoms in the doped samples are also evident from the EDX images of doped ZnO. The calculated quantitative ratio of Ni/Zn are found to be 0.026, 0.042, 0.063, 0.075 and 0.099, respectively, for 2%, 4%, 6%, 8% and 10% Ni doped ZnO which confirms that the Ni atoms are successfully doped in the ZnO host lattice.

Figure 5a–c shows the TEM, HRTEM and SAED image of the undoped, 4% and 8% Ni doped ZnO. TEM image of the pure ZnO shows the formation of the spindle morphology as obtained in SEM. The lattice fringe in HRTEM and bright diffraction spot in the SAED image confirm the crystalline nature of the synthesized sample [23]. In the HRTEM of undoped ZnO, the interplanar spacing is 0.2612 nm which corresponds to the plane (002) of the wurtzite ZnO and is in good agreement as calculated from the XRD (0.2614 nm). Similarly, for 4% and 8% doped ZnO, a lattice plane orienting along (100) and (101), respectively, are seen whose respective d-spacing are 0.2814 nm and 0.2477 nm. The calculated value of these respective d-spacing from the XRD are 0.2816 nm and 0.2473 nm.

The formation of ZnO wurtzite structures in the Ni doped ZnO samples was further supported by FTIR measurements. Similar spectra were observed for the undoped and Ni doped ZnO samples. For all the doped and undoped samples, the broad absorption band at ~ 3400 cm^{-1} is attributed to O–H stretching which arises because of some absorbed moisture. The band at ~ 1642 cm^{-1} can be associated with the bending vibrations of H_2O molecules. The absorption band at ~ 1520 cm^{-1} and 1360 cm^{-1} is due to the carbonyl groups of the carboxylate ions which might remain adsorbed on the surface of ZnO [24]. The absorption band at ~ 400–550 cm^{-1} represents stretching modes of ZnO. The weak absorption bands occurring around 675 cm^{-1} and 1046 cm^{-1} are associated with Ni^{2+} occupation at Zn^{2+} sites. Intrinsic host lattice defects are activated because of the ionic radii mismatch between Ni^{2+} and Zn^{2+} and these types of impurities caused the vibrational mode [25] (Fig. 6).
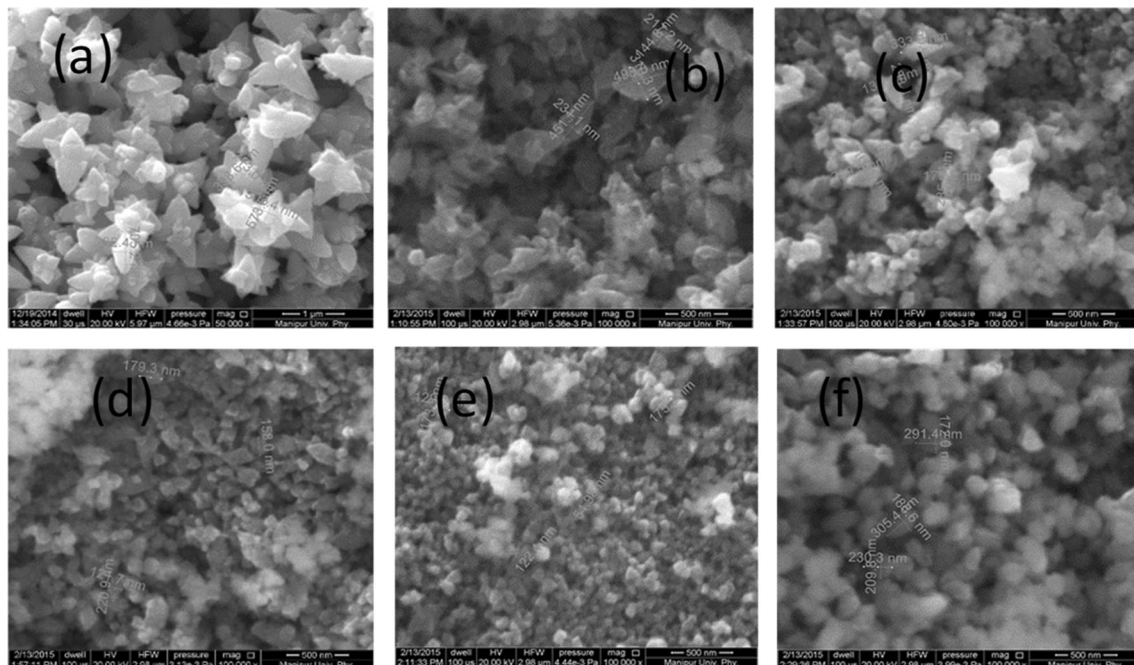
3.3 Optical properties

Figure 7 shows the UV–Visible absorption spectra of undoped and Ni doped ZnO samples. A well excitonic absorption peak which arises due to the optical transition of electron from the valence band to the conduction band of the material is obtained for all samples. From this excitonic absorption peak, the optical band gap energy (E_g) can be calculated using the relation $E_g = hc/\lambda$ where λ is the wavelength of the excitonic absorption peak, h is Planck's constant ($h = 6.62 \times 10^{-34}$ J s) and c is speed of light ($c = 3 \times 10^8$ m s^{-1}) [26]. The wavelength of the excitonic absorption peak and the corresponding band gap energy for the samples are reported in Table 2.

The variation of E_g with Ni concentration is shown in Fig. 8 and is found to vary nonlinearly with the Ni concentration. As can be seen E_g initially drops from 3.54 eV for the undoped sample to 3.11 eV for $x = 0.02$ and then increases upto 3.59 eV for $x = 0.06$. With further increase in dopant concentration it is observed that the band gap decreases to 3.35 eV for $x = 0.1$.

The initial decrease in E_g at low concentration of Ni ions ($x = 0.02$) can be attributed to the strong sp–d

Table 1 Rietveld refined structural parameters for Ni doped ZnO nanoparticles

Compounds	ZnO	$Zn_{0.98}Ni_{0.02}O$	$Zn_{0.96}Ni_{0.04}O$	$Zn_{0.94}Ni_{0.06}O$	$Zn_{0.92}Ni_{0.08}O$	$Zn_{0.90}Ni_{0.1}O$
Crystal system	Hexagonal	Hexagonal	Hexagonal	Hexagonal	Hexagonal	Hexagonal
Space group	$P63mc$ (No. 186)	$P63mc$ (No. 186)	$P63mc$ (No. 186)	$P63mc$ (No. 186)	$P63mc$ (No. 186)	$P63mc$ (No. 186)
Lattice parameters (Å)						
a	3.255 (4)	3.254 (4)	3.254 (4)	3.253 (6)	3.252 (5)	3.252 (1)
c	5.217 (6)	5.218 (6)	5.217 (7)	5.215 (1)	5.214 (9)	5.213 (4)
Cell volume ($Å^3$)	47.86 (9)	47.86 (1)	47.84 (1)	47.79 (5)	47.77 (1)	47.75 (3)
Atomic positions						
Zn/Ni	(2b)	(2b)	(2b)	(2b)	(2b)	(2b)
x	0.3333	0.3333	0.3333	0.3333	0.3333	0.3333
y	0.6666	0.6666	0.6666	0.6666	0.6666	0.6666
z	0.0000	0.0000	0.0000	0.0000	0.0000	0.0000
O	(2b)	(2b)	(2b)	(2b)	(2b)	(2b)
x	0.3333	0.3333	0.3333	0.3333	0.3333	0.3333
y	0.6666	0.6666	0.6666	0.6666	0.6666	0.6666
z	0.3828 (5)	0.3867 (9)	0.3873 (7)	0.3867 (1)	0.3858 (9)	0.3860 (2)
$R_{Factors}$						
R_p	13.0	12.0	11.3	10.7	10.1	10.3
R_{wp}	17.5	16.0	14.6	13.9	13.0	13.2
R_{exp}	14.2	13.4	12.5	11.80	11.07	11.04
χ^2	1.52	1.42	1.34	1.40	1.37	1.43
R_{Bragg}	6.34	6.06	6.78	8.15	7.82	9.50
R_F	4.63	4.35	4.85	5.52	4.98	5.98

Fig. 3 SEM images of **a** undoped ZnO, **b** 2% Ni doped ZnO, **c** 4% Ni doped ZnO, **d** 6% Ni doped ZnO, **e** 8% Ni doped ZnO and **f** 10% Ni doped ZnO samples
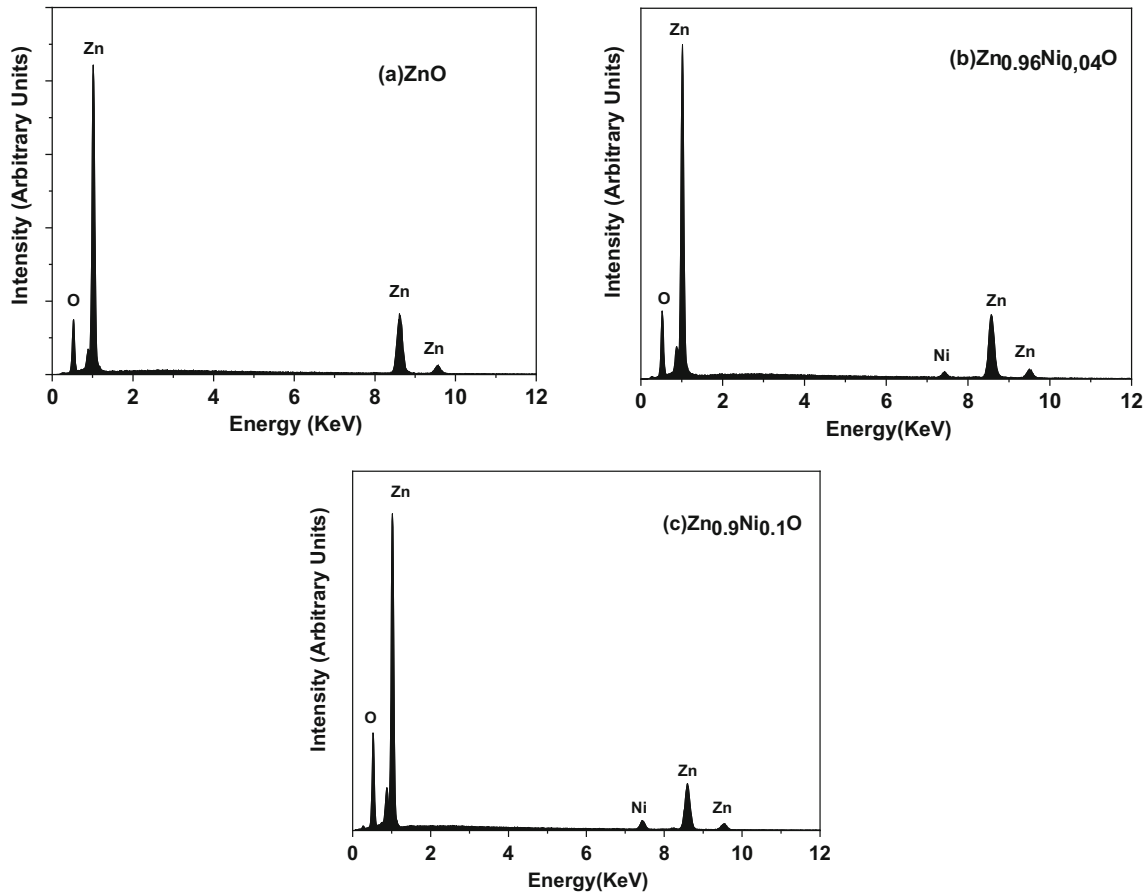
Fig. 4 EDX spectrum of **a** undoped ZnO, **b** 4% Ni doped ZnO and **c** 10% Ni doped ZnO

exchange interaction between the localized d electron of Ni atoms and band electrons of ZnO [27]. As the Ni concentration is increased the BM effect becomes prominent and overcomes the decreasing effect of sp–d exchange interaction, leading to the observed increase in E_g for x upto 0.06 [28]. At still higher concentration of Ni dopant $x > 0.06$, the band gap widening due to the BM band filling effect might have been counteracted by a shrinkage of band gap energy due to the modification of electronic states in the crystal caused by the correlated motion of charge carriers and their scattering against the impurity [29]. This dominant band gap renormalization effect may be responsible for the decreasing behavior of E_g beyond $x = 0.06$. The above discussion on the competitive effect of the three phenomena can be expressed as

$$E_g = E_{g0} - \Delta E_{sp-d} + \Delta E_{BM} - \Delta E_{BGR}, \tag{7}$$

where E_{g0} is the band gap energy of undoped ZnO, ΔE_{sp-d} is band gap narrowing term due to sp–d

exchange interaction, ΔE_{BM} is the band gap widening term due to BM effect and ΔE_{BGR} is the band gap shrinkage term due to band gap renormalization effect. Similar variation in the band gap has also been reported by earlier workers [30–33].
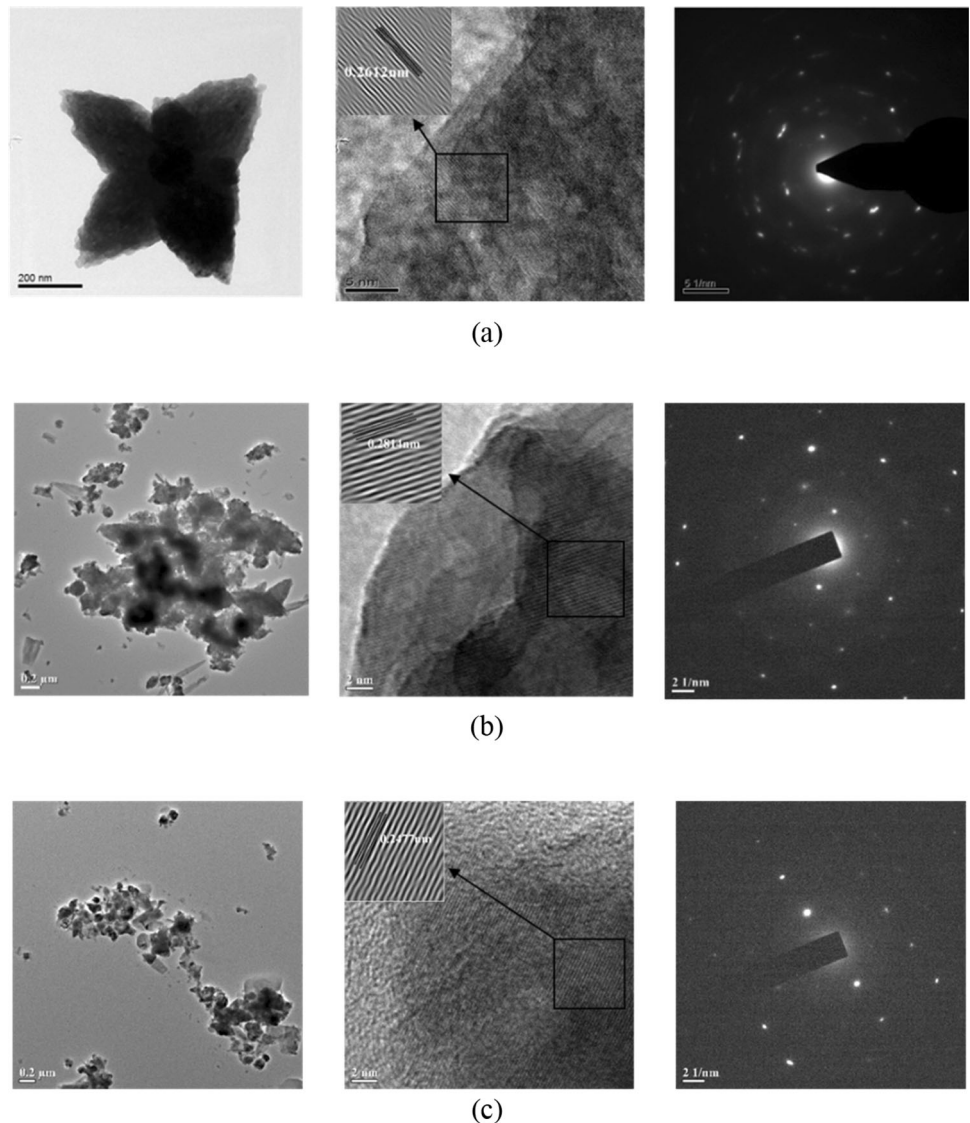
3.4 Photocatalytic study

According to Lambert–Beer law, commonly known as the Beer's law, absorption is directly proportional to concentration. Hence the degradation percentage of the process can be obtained by the relation

$$\%D = \frac{C_0 - C_t}{C_0} \times 100\% = \frac{A_0 - A_t}{A_0} \times 100\%, \tag{8}$$

where $\%D$ is degradation percentage, C_0 is initial concentration before irradiation, C_t is concentration after time t of irradiation, A_0 is absorbance before irradiation, A_t is absorbance after time t of irradiation.

The relationship between degradation percentage and irradiation time is shown in Fig. 9a. It is evident

Fig. 5 TEM, HRTEM image and SAED pattern of **a** undoped ZnO, **b** 4% Ni doped ZnO and **c** 8% Ni doped ZnO

(a)

(b)

(c)

from the graph that the photocatalytic performance is affected by the doping of ZnO with Ni. As seen from the graph, the photocatalytic performance get enhanced upon low level of doping (2%, 4%, 6%), whereas it gets reduced for high level doping i.e., 8% and 10%. The increase in degradation percentage may be due to the reduction in electron-hole recombination as doping of ZnO with transition metals introduces new energy level below the conduction band [34].With further increase in doping concentration beyond 6%, the photocatalytic performance was observed to decrease. This might be due to the creation of excess oxygen vacancies which provides the recombination centers for the electrons and holes [35]. The plot between $\ln(C_0/C)$ and irradiation time (Fig. 9b), with two linear portions, shows that the

photodegradation process follows pseudo first-order reaction [36, 37]. The first linear portion corresponds to the absorption of the dye molecules into the photocatalyst surface forming intermediate species whose rate constant is given by k_1. The degradation of intermediate species into colorless product is indicated by the second plot whose rate constant is k_2 [38, 39].

The values of rate constants for the samples are presented in Table 3.

Maximum photodegradation was observed for $Zn_{0.94}Ni_{0.06}O$ degrading 77% of the dye under 4 h of irradiation. The effects of photocatalyst dosage, initial

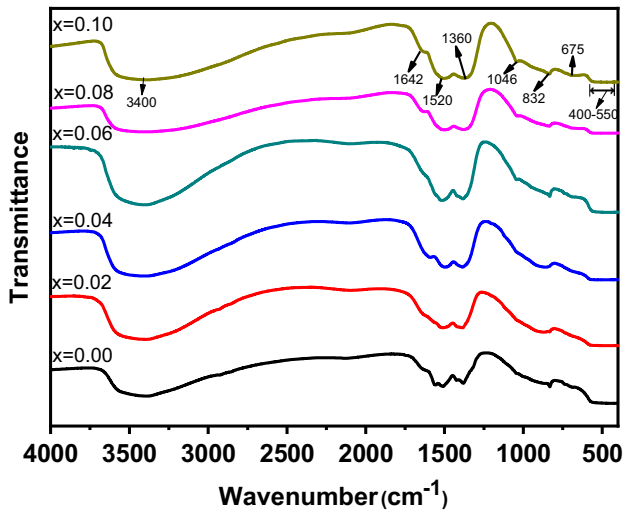**Fig. 6** FTIR spectra of Ni doped ZnO nanoparticles at various concentration. The spectra are shifted vertically for clarity
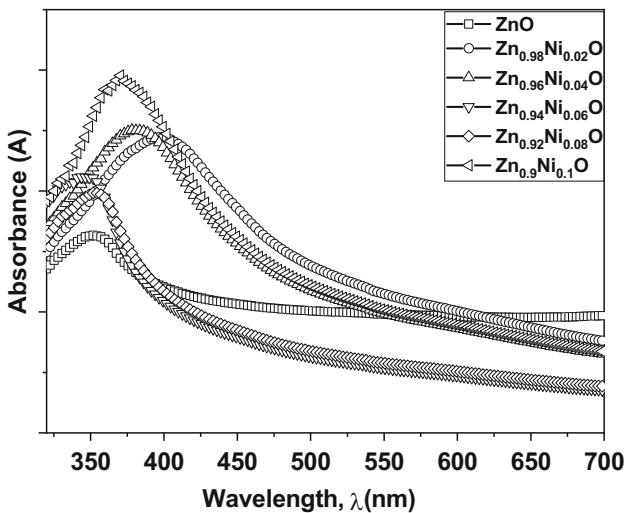

Fig. 8 Variation of band gap energy with Ni concentration

Fig. 7 UV–Visible absorption spectra of undoped and Ni doped ZnO samples

dye concentration and pH were further studied for $Zn_{0.94}Ni_{0.06}O$.

3.4.1 Effect of photocatalyst amount

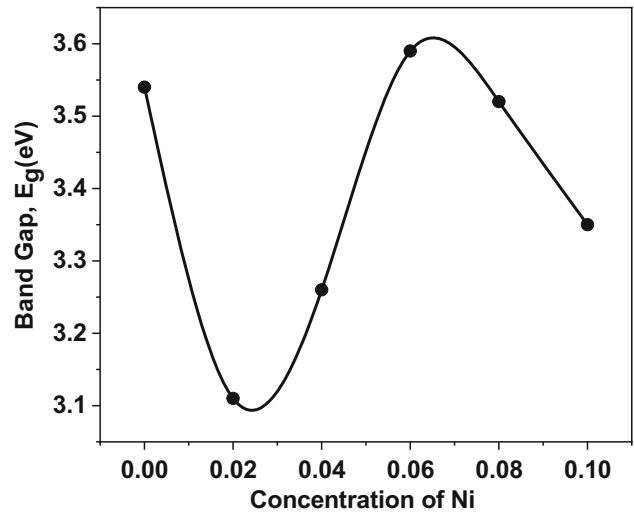Catalyst dosage is one of the main factors that influence the photocatalytic efficiency. Experiments were

performed for different amounts of the sample (0.05 g/L, 0.10 g/L, 0.15 g/L) with fixed value of initial dye concentration and pH at 15 ppm and 7, respectively. The photocatalytic action was first observe to increase with the increase in catalyst amount upto 0.10 g/L by degrading 77% of the dye under 4 h of irradiation which may be attributed to the higher availability of active sites in higher photocatalyst amount. Further increase in the catalyst amount resulted in the decreased photocatalytic activity due to agglomeration of the nanoparticles which might have caused turbidity reducing light penetration due to scattering [40, 41] (Fig. 10).

3.4.2 Effect of initial dye concentration

To examine the influence of initial dye concentration on the degradation percentage, experiments were performed for different concentrations of the dye (10 ppm, 15 ppm and 20 ppm) with catalyst amount and pH fixed at 0.10 g/L and 7, respectively. Their effect and kinetic study are represented in Fig. 11a and b, respectively. The degradation efficiency depends on the probability of reaction between the dye molecules and the catalyst which increases with

Table 2 Value of excitonic absorption peak and band gap energy of undoped and Ni doped ZnO

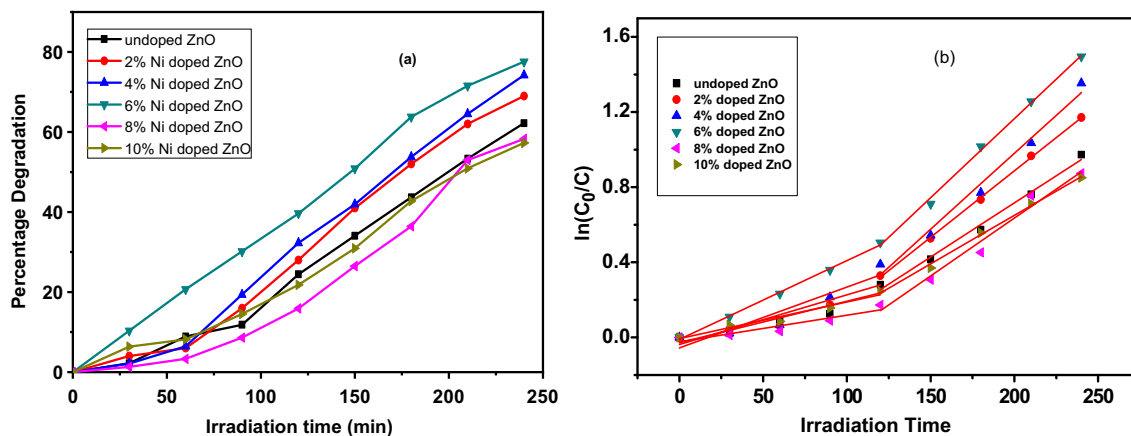| Sample	ZnO	$Zn_{0.98}Ni_{0.02}O$	$Zn_{0.96}Ni_{0.04}O$	$Zn_{0.94}Ni_{0.06}O$	$Zn_{0.92}Ni_{0.08}O$	$Zn_{0.9}Ni_{0.1}O$
Absorption peak (nm)	350.4	398.8	379.8	345.4	352.6	370.3
Band gap (eV)	3.54	3.11	3.26	3.59	3.52	3.35

Fig. 9 **a** %D vs t, and **b** ln(C_0/C) vs t for ZnO, $Zn_{0.98}Ni_{0.02}O$, $Zn_{0.96}Ni_{0.04}O$, $Zn_{0.94}Ni_{0.06}O$, $Zn_{0.92}Ni_{0.08}O$, $Zn_{0.90}Ni_{0.10}O$

increasing dye concentration for fixed amount of the sample. When the dye concentration exceeds a maximum value the excess dye molecules will cover upto the catalyst molecules which inhibits light to reach the sample thereby producing a screen effect [42–44]. Hence photocatalytic activity first increases and then decreases with increase in dye concentration.

3.4.3 Effect of pH

The solution pH is an important parameter affecting the degradation efficiency because it can depict the surface charge behavior of the catalyst which in turn depends on the point zero charge (pzc) of the photocatalyst. Experiments were performed by varying the pH of the solution (5, 7, 9 and 10) using NaOH solution and HCl. ZnO has pzc from 8 to 9 [45]. From Fig. 12a, b it is observed that the photodegradation percentage is less in acidic medium because for pH < pzc, the catalyst surface becomes positively charged which repels dye molecules, since MG is a cationic dye. At pH > pzc, the surface of the catalyst becomes negatively charged which attracts the dye molecule [46, 47]. Optimum degradation is obtained at pH 9 which degrades the dye upto 76% under irradiation time of 1 h.

3.5 Confirmation of photocatalysis mechanism

In order to investigate the mechanism of the photodegradation process, experiments were performed for the following cases.

a. With catalyst under light irradiation (photocatalysis).
b. With catalyst under dark.
c. Without catalyst under light (photolysis).

As shown in Fig. 13, almost no degradation of the dye was observed for the cases of photolysis and experiment with catalyst under dark and degradation was observed only for the experiment with catalyst under light irradiation. This confirms that the degradation process is the combined effect of both light and catalyst as mentioned before in the mechanism of photocatalysis.

3.6 Reusability test for photocatalyst

A stable and reusable photocatalyst is of great importance for the long-term application of the sample. Stability of the sample was investigated for three consecutive runs of the photocatalytic experiment. After each run, the catalyst was washed four times with distilled water, collected and dried in hot air oven at 50 °C for 48 h. It was observed that some
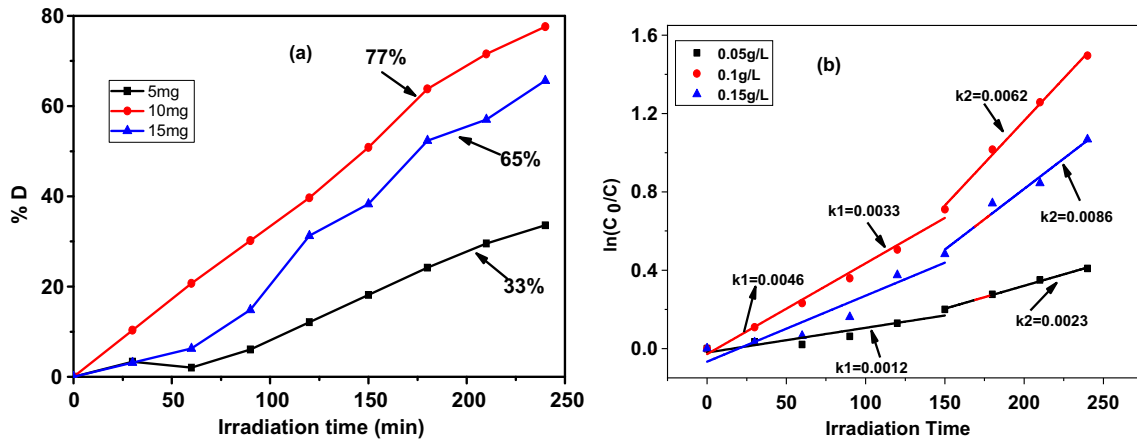
Table 3 Rate constants for $Zn_{1-x}Ni_xO$ (x = 0.00, 0.02, 0.04, 0.06, 0.08 and 0.10)

Sample	ZnO	$Zn_{0.98}Ni_{0.02}O$	$Zn_{0.96}Ni_{0.04}O$	$Zn_{0.94}Ni_{0.06}O$	$Zn_{0.92}Ni_{0.08}O$	$Zn_{0.90}Ni_{0.10}O$
k_1	0.0022	0.0026	0.0032	0.0042	0.0014	0.0019
k_2	0.0057	0.007	0.0080	0.0084	0.0061	0.0051

Fig. 10 **a** %*D* vs. *t*, and **b** $\ln(C_0/C)$ vs *t* for different catalyst loading of 0.05 g/L, 0.10 g/L, 0.15 g/L at initial dye concentration of 15 ppm and pH 7 for $Zn_{0.94}Ni_{0.06}O$
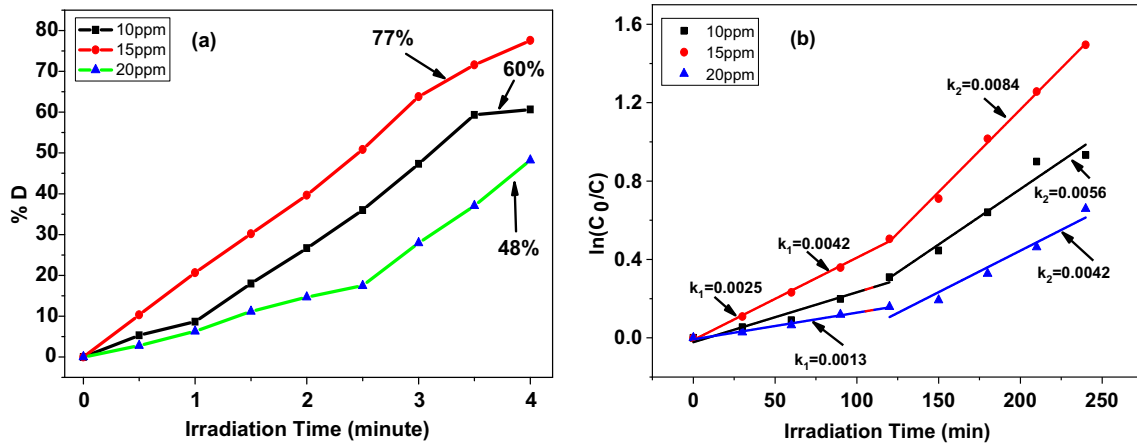

Fig. 11 **a** %*D* vs. *t* and **b** $\ln(C_0/C)$ vs *t* for different initial dye concentration of 10 ppm, 15 ppm and 20 ppm with fixed catalyst amount of 0.10 g/L and pH 7 for $Zn_{0.94}Ni_{0.06}O$

amount of the catalyst was lost after recollection. Initially, 10 mg was used after which 6.8 mg and then 4.5 mg of the catalyst was recollected after each run. This may be due to the small size of the nanoparticle and there might be some loss during washing process. After the third run, it was observed that the photodegradation efficiency decreases from 75 to 34.21% at the same experimental conditions. The decreased in degradation efficiency might be due to the adsorption of some byproducts of the dye into the pores and cavities of the photocatalyst which reduces the active sites of the process [48, 49] thereby resulting in the decrease production of the radicals necessary for the photocatalytic degradation of the dye. This is one of the major drawbacks for the use of nanomaterials for degradation process in the large-scale and long-term application. It may be overcome

by immobilizing the nanoparticles on a supporting medium such as polymer which will also solve the problem in recollection of the sample (Fig. 14).

4 Conclusions

To summarize, undoped and Ni doped ZnO (with different doping concentrations) were synthesized using chemical precipitation method and their structural, optical, morphological and photocatalytic properties were examined. 6% Ni doped ZnO was observed to be the most efficient catalyst which degrades 77% of the dye under 4 h of UV irradiation. At the optimal condition of photocatalyst dosage 0.1 g/L, 15 ppm of dye concentration and pH 9, 76%
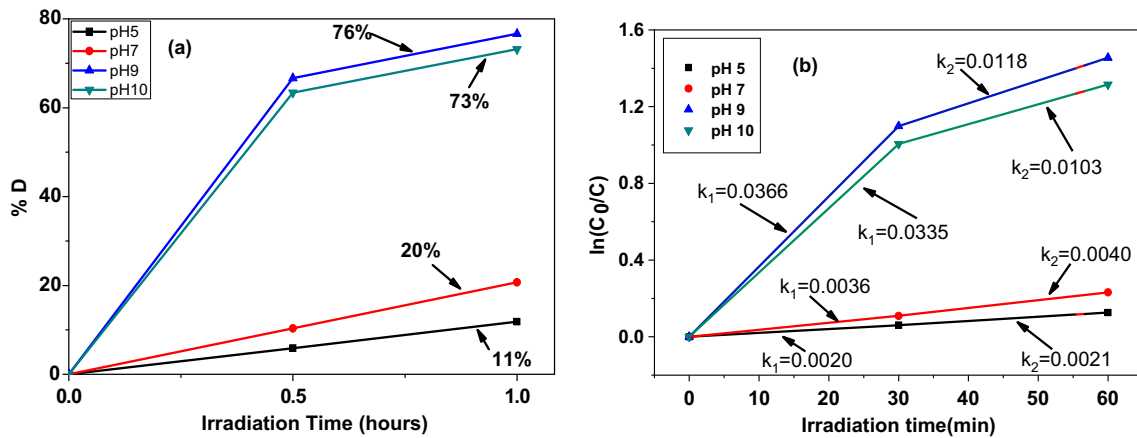
Fig. 12 **a** %D vs. t and **b** ln(C$_0$/C) vs t for different pH of the solution of 5, 7, 9 and 10 with fixed catalyst amount of 0.10 g/L and initial dye concentration of 15 ppm for Zn$_{0.94}$Ni$_{0.06}$O
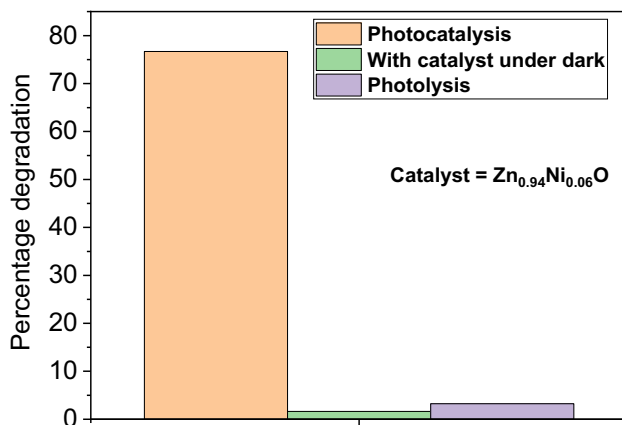

Fig. 13 Degradation of MG dye with catalyst under light, with catalyst under dark, without catalyst under light
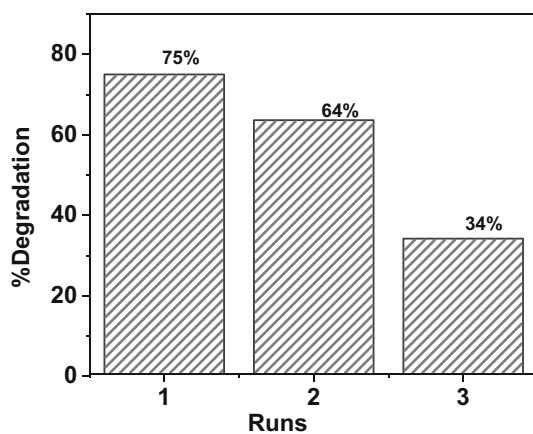

Fig. 14 Reusability of Zn$_{0.94}$Ni$_{0.06}$O photocatalyst for three consecutive cycles for the degradation of MG

of the dye was degraded under 1 h of UV irradiation. We have observed that the enhanced photocatalytic action of the Ni doped ZnO is attributed to the decrease in electron–hole recombination which increases the formation of radicals resulting in higher photocatalytic degradation of the dye. Investigation of different experimental conditions shows the degradation activity is the combined effect of both light and the photocatalyst and not the individual effect. Checking of the reusability of the catalyst results in the decrease in degradation efficiency due to absorption of byproducts.

Acknowledgements

References

1. M.M. Sajid, S.B. Khan, N.A. Shad, N. Amin, Z. Zhang, RSC Adv. **8**, 23489–23498 (2018)
2. S.G. Babu, P. Karthik, M.C. John, S.K. Lakhera, M. Ashokkumar, J. Khimd, B. Neppoliana, Ultrason. Sonochem. **50**, 218–223 (2019)
3. C.B. Ong, L.Y. Ng, A.W. Mohammad, Renew. Sustain. Energy Rev. **81**, 536–551 (2018)
4. Z.L. Wang, J. Phys. Condens. Matter **16**, R829 (2004)

5. R.S. Sabry, W.J. Aziz, M.I. Rahmah, J. Inorg. Organomet. Polym. Mater. **30**, 4533–4543 (2020)

6. R.S. Sabry, M.I. Rahmah, W.J. Aziz, J. Mater. Sci. Mater. Electron. **31**, 13382–13391 (2020)

7. X. Cai, Y. Cai, Y. Liu, H. Li, F. Zhang, Y. Wang, J. Phys. Chem. Solids **74**(9), 1196–1203 (2013)

8. W. Jing, Z. Li, X.Y.Y. Yang, Y. Lei, J. Zhou, Y. Huang, Y. Gu, Y. Zhang. Mater. Res. Bull. **46**, 1207–1210 (2011)

9. S.M. Mousavi, A.R. Mahjoub, R. Abazari, J. Mol. Liq. **242**, 512–519 (2017)

10. S. Kant, A. Kumar, Adv. Mater. Lett. **3**(4), 350–354 (2012)

11. A.K. Azfar, M.F. Kasim, I.M. Lokman, H.A. Rafaie, M.S. Mastuli, R. Soc. Open Sci. **7**, 191590 (2020)

12. A.I. Md., I. Molla, M. Tateishi, H. Furukawa, T. Katsumata, S. Suzuki, Kaneco, Open J. Inorg. Non-met. Mater. **7**, 1–7 (2017)

13. I.M.P. Silva, G. Byzynski, C. Ribeiro, E. Longo, J. Mol. Catal. A **417**, 89–100 (2016)

14. N. Kumaresan, K. Ramamurthi, R.R. Babu, K. Sethuraman, S.M. Babu, Appl. Surf. Sci. **418**, 138–146 (2017)

15. B.D. Culity, *Elements of X-Ray Diffraction* (Addison-Wesley Publishing Company, Inc., Reading, 1956), p. 99

16. V. Gandhi, R. Ganesan, H. Hameed, A. Rahman, M. Thaiyan, J. Phys. Chem. C **118**, 9715 (2014)

17. K. Raja, P.S. Ramesh, D. Geetha, Spectrochim. Acta A **120**, 19 (2014)

18. J. Rodriguez-Carvajal, *FULLPROF 2000: A Rietveld Refinement and Pattern Matching Analysis Program* (Laboratoire Léon Brillouin (CEA-CNRS), France, 2008).

19. A.J. Reddy, M.K. Kokil, H. Nagabhushan, J.L. Rao, C. Shivakumara, B.M. Nagabhushana, R.P.S. Chakradhar, Spectrochim. Acta A **81**, 53 (2011)

20. V. Kumar, S. Kumari, P. Kumar, M. Kar, L. Kumar, Adv. Mater. Lett. **6**(**2**), 139 (2015)

21. Y. Du, J. Fang, M. Zhang, J. Hong, Z. Yin, Q. Zhang, Mater. Lett. **57**, 802 (2002)

22. M.L. Moreira, S.A. Pianaro, A.V.C. Andrade, A.J. Zara, Mater. Charact. **57**, 193 (2006)

23. F.R. Egerton, *Physical Principles of Electron Microscopy* (Springer, New York, 2005), p. 112

24. R. Saravanana, K. Santhia, N. Sivakumar, V. Narayanan, A. Stephena, Mater. Charact. **67**, 10 (2012)

25. C.K. Ghosh, S. Malkhandi, M.K. Mitra, K.K. Chattopadhyay, J. Phys. D **41**, 245113 (2008)

26. L.S. Devi, K.N. Devi, B.I. Sharma, H.N. Sarma, Indian J. Phys. **88**, 477 (2014)

27. S.V. Bhat, F.L. Deepak, Solid State Commun. **135**, 345 (2005)

28. E. Burstein, Phys. Rev. **93**, 632 (1954)

29. B.E. Sernelius, K.F. Berggren, Z.C. Jin, I. Hamberg, C.G. Granqvist, Phys. Rev. B. **37**, 10244 (1988)

30. S. abed, M.S. Aida, K. Bouchouit, A. Arbaoudi, K. Iliopus, B. Sahraoui, Opt. Mater. **33**, 968 (2011)

31. K.H. Naeem-ur-Rehman, M. Mehmood, F. Ali, M.A. Rasheed, M. Younas, F.C.C, Ling, S.M. Ali, Chem. Phys. Lett. **651**, 35 (2014)

32. K. Tang, S. Gu, J. Liu, J. Ye, S. Zhu, Y. Zheng, J. Alloys Compd. **653**, 643 (2015)

33. H.S. Al-Salman, M.J. Abdullah, Superlattice Microstruct. **60**, 349 (2013)

34. Y.G. Habba, M.C. Gnambodoe, Y.L. Wang, Appl. Sci. **7**, 1185 (2017)

35. L.A. Chanu, W.J. Singh, K.J. Singh, K.N. Devi, Results Phys. **12**, 1230–1237 (2019)

36. D. Das, P. Mandal, RSC Adv. **6**, 6144–6153 (2016)

37. G. Vijayaprasath, R. Murugan, S. Asaithambi, P. Sakthivel, T. Mahalingam, Y. Hayakawa, G. Ravi, Ceram. Int. **42**, 2836–2845 (2016)

38. M.V. Limaye, S.B. Singh, R. Das, P. Poddar, S.K. Kulkarni, J. Solid State Chem. **184**, 391–400 (2011)

39. C.H. Ahn, Y. Yi Kim, D.C. Kim, S.K. Mohanta, H.K. Cho, J. Appl. Phys. **105**, 089902 (2009)

40. A.J. Reddy, M.K. Kokila, H. Nagabhushana, J.L. Rao, C. Shivakumara, B.M. Nagabhushana, R.P.S. Chakradhar, Spectrochim. Acta A **81**, 53–58 (2011)

41. A. Ajmal, I. Majeed, R.N. Malik, H. Idriss, M.A. Nadeem, RSC Adv. **4**, 37003–37026 (2014)

42. C.M. So, M.Y. Cheng, J.C. Yu, P.K. Wong, Chemosphere **46**, 905–912 (2002)

43. S. Sakthivel, B. Neppolian, M.V. Shankar, B. Arabindoo, M. Palanichamy, V. Murugesan, Sol. Energy Mater. Sol. Cells **77**, 65–82 (2003)

44. K.N. Devi, W.J. Singh, K.J. Singh, *PFAM-XXVI*, pp. 725–736 (2017)

45. K.M. Reza, A.S.W. Kurny, F. Gulshan, Appl. Water Sci. **7**, 1569–1578 (2017)

46. M. Kosmulski, J. Colloid Interface Sci. **298**, 730–741 (2006)

47. A. Gupta, J.R. Saurav, S. Bhattacharya, RSC Adv. **5**, 71472–71481 (2015)

48. A.N. Ejhieh, S. Khorsandi, J. Ind. Eng. Chem. **20**(3), 937–946 (2014)

49. B. Shahmoradi, F. Farahani, S. Kohzadi, A. Maleki, M. Pordel, Y. Zandsalimi, Y. Gong, J. Yang, G. McKay, S.M. Lee, J.K. Yang, Water Sci. Technol. **79**(2), 375–385 (2019)